 CMES, vol.79, no.1, pp.63-82, 2011

Predictions of Lid-Driven Flow in a Two-Dimensional Irregular Cavity: a Numerical Study

Bruno Manoel Pasquim[1] **and Viviana Cocco Mariani**[1]

Abstract: The main aim of this study was to evaluate the capacity of a Eulerian-Lagrangian methodology (ELAFINT) to accurately deal with incompressible viscous steady flow in a domain with corners and curved boundaries. Thus, a two-dimensional lid-driven cavity with an irregular bottom was selected. The equations that govern the flow are discretized using the finite-volume method with a Cartesian grid. The evolution of the velocity fields, stream function and vorticity in the irregular cavity when the Reynolds number increases from 500 to 6000 is captured by the method under investigation. The results show that with an increase in the Reynolds number there is the development of new vortices in the flow and also a reduction in the kinetic energy.

Keywords: Triangular cavity, Cartesian grid, Eulerian-Lagrangian methodology, finite-volume method

1 Introduction

Lid-driven cavity flow has been extensively studied due to its relevance to a great number of engineering applications, such as solar collectors, enhanced thermal performance of heat exchangers, bearings and lubrication systems. A detailed review of previous studies on lid-driven cavity flows can be found in Chang and Cheng (1999), Chen and Cheng (2002).

The flow in square cavities is referenced to exemplify many types of flow and is also used as a model to test flow precision. Numerical methods used to solve square lid-driven cavity flow can not be applied without modification to triangular and trapezoidal cavities, geometries which are common in nature.

The fact that the numerical methods for the resolution of square cavities can not be applied to irregular cavities is due to the special attention that has been given to

[1] Department of Mechanical Engineering, Pontifical Catholic University of Parana, Rua Imaculada Conceicao, 1155, Prado Velho, 80215-901, Curitiba, PR, Brazil {bpasquim@hotmail.com; viviana.mariani@pucpr.br}

flow boundaries. Thus, for example, the classic finite-volume method, using structured meshes, needs to be modified in order to solve the flow for these geometries. The differences between the numerical solutions for square cavities and triangular cavities have led to new studies and the development of new numerical methods which are more reliable and accurate for the solution of flows in irregular cavities.

The representation of two-dimensional cavities of square sections with infinite axial length has been widely studied and has become a standard test case for new computational schemes. Relevant studies in this context include Benjamin and Denny (1979), Ghia et al. (1982), Botella and Peyret (1998), and Bruneau and Saad (2006). These authors employed the finite-difference method with a stream function-vorticity formulation, with the exception of the latter in which uniform Cartesian meshes were used.

Some recent studies solving flows in lid-driven cavities have used meshless methods. One popular approach is the meshless local Petrov-Galerkin (MLPG) method, successfully used by Lin and Atluri (2001) and Ahrem et al. (2006). Arefmanesh et al. (2008, 2010) applied the MLPG method to solve non-isothermal lid-driven cavity flow. Tsai et al. (2002) developed a meshless boundary elements method to solve 3D Stokes flows. The iterative process used therein is similar to the process employed in Nicolás and Bermúdez (2007), the only difference being that the former used a truly fixed point, with a different discretization time, while Nicolás and Bermúdez (2004) studied the 2D flows.

Radial basis functions (RBFs) are a powerful tool for function interpolation. Due to their mesh-free nature RBFs have received increasing attention in relation to solving partial differential equations. This approach was tested by Atluri et al. (2006a, 2006b), Han et al. (2006), Wen and Hon (2007) and Mai-Duy et al. (2007). A new numerical scheme based on Cartesian grids and local integrated radial-basis-function networks (IRBFNs) was employed for the solution of second-order elliptic differential problems defined on two-dimensional regular and irregular domains in Mai-Duy and Tran-Cong (2009).

Another approach is the Multiquadric Collocation Method (MCM) using a radial basis function, which has been used in a variety of studies including some on the lid-driven cavity flows. For example, Ding et al. (2006) used MCM to solve the three-dimensional lid-driven cavity flow problem. Young et al. (2004) solved the problem of Stokes flow in a cavity by MCM. Chantasiriwan (2006) reports driven cavity results for a low Reynolds number ($Re = 0$), which turns out to be a Stokes flow because of the infinity viscosity, and $Re = 100$ using a MCM. Mai-Duy and Tran-Cong (2004) with the primitive variables formulation, also reported the lid-driven cavity flow for $Re = 100$ and $Re = 0$, where Re is the Reynolds number. Grimaldi et al. (2006) using a parallel multi-block method reported results for 2D

and 3D lid-driven cavity problems. Orsini et al. (2008) presented a modified control volume method using a radial basis function interpolation to improve the accuracy of the prediction of the flux at the faces of the control volumes. The proposed approach validated a series de 1D and 3D test cases. Shan et al. (2008) numerically studied the performance of the 3D local multiquadric-based differential quadrature (MQ-DQ) method and demonstrated its capability and flexibility in the simulation of 3D incompressible fluid flows with curved boundary. A new meshless approach was proposed by Mai-Cao and Tran-Cong (2008) in order to solve a special class of moving interface problems. Sellountos and Sequeira (2008) proposed a hybrid velocity-vorticity scheme for the solution of the 2D Navier-Stokes equations. Mariani et al. (2008) investigated Voronoi unstructured meshes to solve the flow in square lid-driven cavities.

In irregular cavities, such as trapezoidal, semi-circular or triangular cavities, special attention has been given to boundaries, for example, the classic finite-volume method, using structured meshes, needs to be modified in order to solve the flow in these geometries. These differences promote the development of research studies and new numerical methods which are faster and more accurate for the solution of flows in irregular geometries.

In the literature there are reports of studies on the flow in curved and non-rectangular cavities. The triangular cavity exhibits flow features that have been analytically studied by Moffat (1963) in the Stokes regime and by Batchelor (1956) in the inviscid or infinite Reynolds number regime. The flow in a trapezoidal cavity has been studied by Darr and Vanka (1991). Ribbens et al. (1991) described the flow in an elliptic region with a moving boundary. McQuain et al. (1994) and Ribbens et al. (1994) studied the steady flow in an equilateral triangular cavity for $Re \leq 500$. The fourth-order Navier-Stokes equations in terms of stream function were solved numerically using finite differences together with a Newton-like iteration on a transformed geometry. Vynnycky and Kimura (1994) have reported the results for a study on steady flow in a driven quarter circular cavity.

Jyotsna and Vanka (1995) studied the steady viscous flow in a triangular cavity, where triangular grids and a multigrid method were used. The solution for $Re \leq 800$ was obtained without encountering any of the difficulties reported for structured grid-based methods in Ribbens et al. (1994). Li and Tang (1996) presented an accurate and efficient numerical method to solve the flow in equilateral and scalene triangular cavities for $Re \leq 1500$, using finite difference on a transformed geometry. Recently, Glowinski et al. (2006) reported results for a study on incompressible viscous flow in a semi-circular cavity. The operator-splitting/finite elements method and a triangulation of the two-dimensional domain were used to obtain numerical results. The Lattice Boltzmann method was investigated by Duan

and Liu (2007) to solve triangular cavity flow for $Re \leq 500$.

Natural convection within a cavity has received significant attention recently. The pattern of the natural periodic flow motion in a lid-driven triangular cavity was confirmed by Chen and Cheng (2009). Basak et al. (2009) studied the heat flow pattern in triangular cavities using Bejan's heatline concept, as did Kaluri et al. (2010). The unsteady natural convection in a triangular enclosure was investigated by Saha (2011).

In fact, the flow in curved geometries can be represented using curvilinear and non-orthogonal grids or orthogonal (Cartesian) grids. In this context, our primary goal here was to investigate the ability of the finite volume/Eulerian-Lagrangian technique using Cartesian grids as discussed in Ye et al. (1999), Mariani and Prata (2008) and Pasquin and Mariani (2008) to deal with flow regions with corners and curved boundaries. To achieve this goal, we selected a lid-driven irregular cavity flow. This problem is important and of considerable interest because irregular shapes are at least as common in practice as the square shape. Also, we determined which aspects of the results of this problem differ from those of the previously employed method. A secondary goal was to determine the structure of the recirculating flow for Reynolds numbers of between 1and 6000.

The paper is organized as follows. Section 2 introduces the formulation of the problem and shows the boundary conditions of the cavity. Numerical results are presented in Section 3, streamlines and vorticity contours are presented for Re $\leq$ 6000 in the same section. In the last section the main conclusions are detailed.

2 Mathematical Formulation

Figure 1 shows the physical model of an irregular cavity with a constant lid, in which H (= 1 m) and L (= 1 m) indicate the height and width of the cavity, respectively.

The flow considered here is steady, two-dimensional, laminar and incompressible. The air in the cavity is treated as a Newtonian fluid and the fluid properties are assumed to be constant. In this study, the mathematical model is formulated using the continuity and Navier-Stokes equations which can be expressed in Cartesian coordinates (x, y) as (Fox and Macdonald, 2001):

$$\frac{\partial u}{\partial x} + \frac{\partial v}{\partial y} = 0, \tag{1}$$

$$\frac{\partial (uu)}{\partial x} + \frac{\partial (vu)}{\partial y} = -\frac{\partial p}{\partial x} + \nu \left[\frac{\partial^2 u}{\partial x^2} + \frac{\partial^2 u}{\partial y^2} \right], \tag{2}$$

$$\frac{\partial(uv)}{\partial x}+\frac{\partial(vv)}{\partial y}=-\frac{\partial p}{\partial y}+\nu\left[\frac{\partial^2 v}{\partial x^2}+\frac{\partial^2 v}{\partial y^2}\right], \tag{3}$$

where u (m/s) and v (m/s) are the velocity components in the x and y directions, respectively, ν (m^2/s) and p (Pa) are the dynamic viscosity and pressure, respectively.

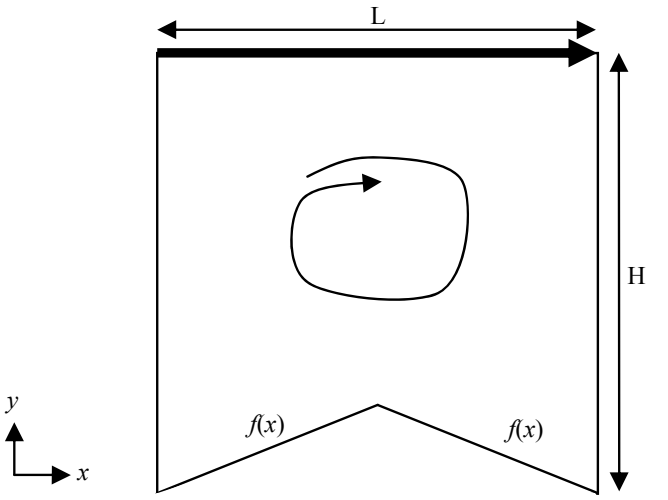

Figure 1: Irregular cavity.

The boundary conditions for the velocity components are given as:

$u = 1$, $v = 0$ for $y = \mathrm{H}$ and $0 \leq x \leq \mathrm{L}$;

$u = 0$,$v = 0$ *for* $0 \leq y \leq \mathrm{H}$ and $x = 0$;

$u = 0$, $v = 0$ for $y = f(x) = 0.4x$ and $0 \leq x \leq \mathrm{L}/2$.

$u = 0$, $v = 0$ for $y = f(x) = -0.4x + 0.4$ and $\mathrm{L}/2 < x \leq \mathrm{L}$.

$u = 0$, $v = 0$ for $0 \leq y \leq \mathrm{H}$ and $x = 0$;

Equations (1) through (3) can be expressed by a single equation for the generic variable ϕ as,

$$\frac{\partial(\rho u\phi)}{\partial x}+\frac{\partial(\rho v\phi)}{\partial y}=\Gamma^{\phi}\frac{\partial}{\partial x}\left(\frac{\partial\phi}{\partial x}\right)+\Gamma^{\phi}\frac{\partial}{\partial y}\left(\frac{\partial\phi}{\partial y}\right)+S^{\phi} \tag{4}$$

where ϕ is equal to u and v for Eqs. (2) and (3), respectively, and unity for Eq. (1), and Γ^{ϕ} and S^{ϕ} are, respectively, the diffusion coefficient and term source. The governing equation, Eq. (4) and its respective boundary conditions were discretized

using the finite-volume method described by Patankar (1980). The irregular cavity is divided into small control volumes using a collocated (non-staggered) arrangement and the Eulerian-Lagrangean method (ELAFINT) as described in Pasquim and Mariani (2008) and Mariani and Prata (2008). The validation of the ELAFINT methodology used in this study was also carried out in Pasquim and Mariani (2008), and the results for an equilateral triangular cavity were compared with those reported in Li and Tang (1996) and McQuain *et al.* (1994), with good agreement.

3 Numerical Results and Discussion

This section, which presents the results for several cavity configurations, is divided into three parts. Presented first is the mesh refinement study. Secondly, the results for the stream function, vorticity, kinetic energy and entropy, i.e., local and global quantities, respectively, are reported and discussed. Finally, the results for the streamlines and vorticity contours are presented and discussed.

3.1 Mesh Refinement Study

Mesh refinement was performed for all cavity configurations investigated. The analysis was based on the velocity profiles along the vertical and horizontal center lines. Four different grids, composed of 50×50, 100×100, 150×150, and 200×200 control volumes, were used as illustrated in Figures 2 and 3.

Figures 2 and 3 present the u and v velocity profiles at the vertical and horizontal center lines, respectively, for a Reynolds numbers of 2500 (Figure 2) and 5000 (Figure 3). The curves for the other configurations investigated are not shown, however, they were similar to those shown in Figures 2 and 3. Since the differences between the results obtained with grids formed of 100×100, 150×150, and 200×200 volumes were minor we chose the 150×150 grid for all the simulations presented in this article.

After choosing the computational grid of 150x150 control volumes, the velocity profiles u and v were built for Reynolds numbers of 500 to 6000 (Figures 4 and 5). The velocity profiles show the evolution of the primary vortex lowering with an increase of Reynolds number, see Figures 4a and 4b. The highest flow velocities are located on the right side of the irregular cavity, see Figures 5a and 5b. The plotted values for the $u-$velocity profiles, along the vertical center line of the irregular cavity, $x = 0.5$, are shown in Table 1, while those for the v-velocity profiles, along the horizontal center line of cavity, $y = 0.5$, are shown in Table 2.

Table 1: Selected numerical values of the u-velocity component along the vertical central line.

Y	Re = 500	Re = 1000	Re = 2000	Re = 3000	Re = 4000	Re = 5000	Re = 6000
0.06333	0	0	0	0	0	0	0
0.13000	0	0	0	0	0	0	0
0.19667	0	0	0	0	0	0	0
0.26333	-0.2571	-0.3443	-0.3885	-0.3857	-0.3719	-0.3557	-0.3383
0.33000	-0.3439	-0.4023	-0.3813	-0.3474	-0.3203	-0.2986	-0.2805
0.39667	-0.3545	-0.3367	-0.2848	-0.2567	-0.2371	-0.2215	-0.208
0.46333	-0.2888	-0.2369	-0.2034	-0.185	-0.1711	-0.1598	-0.1498
0.53000	-0.1894	-0.1474	-0.126	-0.1137	-0.1049	-0.0978	-0.0916
0.59667	-0.088	-0.0602	-0.0463	-0.0405	-0.037	-0.0344	-0.0323
0.66333	0.01229	0.03042	0.03668	0.03601	0.03418	0.03215	0.03005
0.73000	0.11464	0.12746	0.12475	0.11748	0.1102	0.10345	0.09699
0.79667	0.21518	0.2328	0.22144	0.20671	0.19357	0.18192	0.17094
0.86333	0.30438	0.33568	0.32791	0.30794	0.28924	0.27262	0.25705
0.93000	0.44264	0.42371	0.41298	0.3952	0.37563	0.35689	0.33876
0.99667	0.96768	0.95792	0.94048	0.924	0.90821	0.89292	0.87752

Table 2: Selected numerical values of the v-velocity component along the horizontal central line.

x	Re = 500	Re = 1000	Re = 2000	Re = 3000	Re = 4000	Re = 5000	Re = 6000
0.06333	0.08445	0.07126	0.04209	0.02296	0.00703	-0.00996	-0.03534
0.13000	0.14877	0.17761	0.19882	0.19651	0.18468	0.16773	0.14011
0.19667	0.20954	0.27228	0.30327	0.29975	0.28943	0.27791	0.26439
0.26333	0.24887	0.30119	0.3039	0.29188	0.28186	0.27518	0.27396
0.33000	0.24786	0.26203	0.24061	0.22662	0.21812	0.21349	0.21518
0.39667	0.20641	0.18935	0.16847	0.15999	0.15499	0.1523	0.15384
0.46333	0.13757	0.11222	0.10171	0.09835	0.09666	0.09624	0.09871
0.53000	0.05596	0.03755	0.0352	0.03634	0.03806	0.04021	0.04406
0.59667	-0.03059	-0.03776	-0.03354	-0.02754	-0.02209	-0.0171	-0.01152
0.66333	-0.12313	-0.11594	-0.10536	-0.09423	-0.0848	-0.07672	-0.06911
0.73000	-0.22904	-0.19987	-0.18007	-0.16426	-0.15086	-0.13957	-0.12965
0.79667	-0.34359	-0.30609	-0.25845	-0.2361	-0.21928	-0.20531	-0.19338
0.86333	-0.38524	-0.43304	-0.37809	-0.32855	-0.29612	-0.27381	-0.25759
0.93000	-0.22126	-0.32174	-0.42221	-0.4493	-0.44619	-0.43126	-0.41219
0.99667	-0.00572	-0.00502	-0.00264	-0.00042	0.00144	0.00304	0.00454

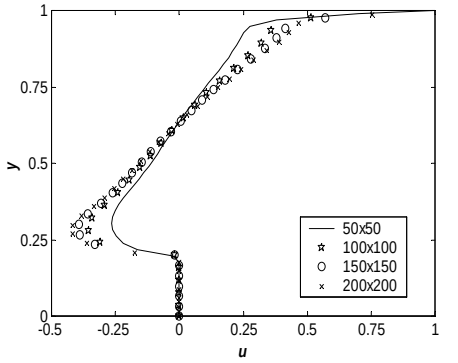

(a)

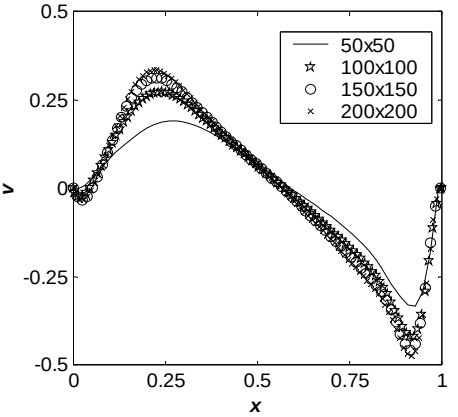

(b)

Figure 2: Profiles of (a) u-velocity along the vertical center line and (b) $v-$velocity along the horizontal center line, for Re = 2500.

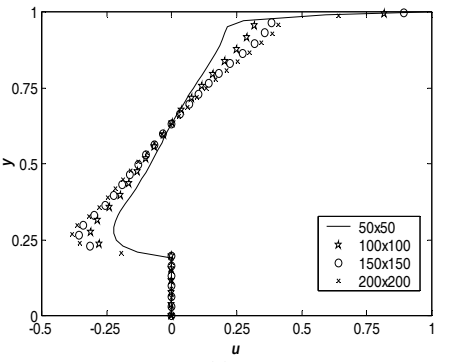

(a)

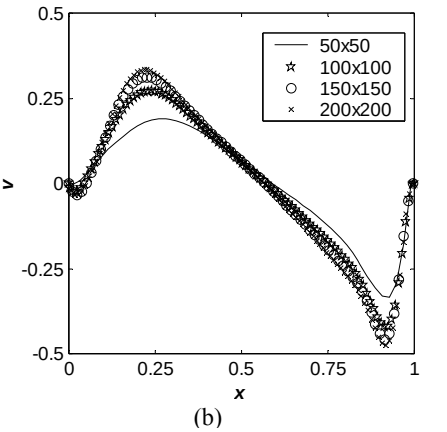

(b)

Figure 3: Profiles of (a) u-velocity along the vertical center line and (b) v-velocity along the horizontal center line, for Re = 5000.

3.2 Analysis of local and global quantities

The analysis of the flow was also based on the stream function, vorticity, kinetic energy and entropy, which were defined as follows. The streamlines describe the vector fields (u, v) for a simple scalar value, ψ. The relationship between the velocity and the stream function is based in the equation of mass conservation, Eq. (1), and is given by,

$$u = \frac{1}{\rho}\frac{\partial \psi}{\partial y}, \tag{5}$$

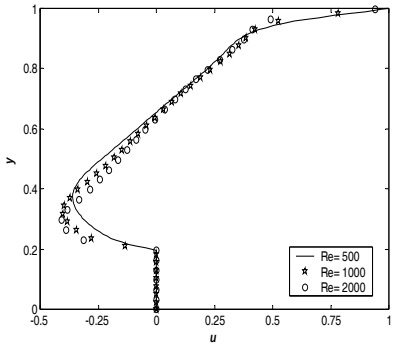

(a)

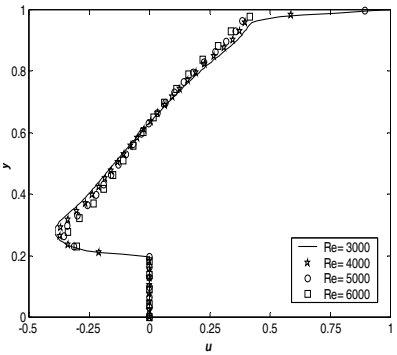

(b)

Figure 4: Profiles of u-velocity along the vertical center line of the cavity for different Reynolds numbers.

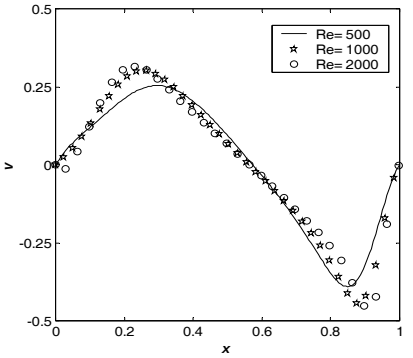

(a)

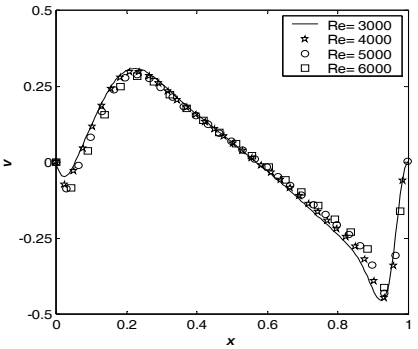

(b)

Figure 5: Profiles of $v-$velocity along the horizontal center line of the cavity for different Reynolds numbers.

$$v = -\frac{1}{\rho}\frac{\partial \psi}{\partial x}. \tag{6}$$

The values of line ψ constant are streamlines, i.e., are lines parallel to velocity vector. The vorticity, ζ, is twice the angular velocity of air at any point, represented by,

$$\zeta = \frac{\partial v}{\partial x} - \frac{\partial u}{\partial y}. \tag{7}$$

The vorticity is a measure of fluid rotation, as it moves in the flow field. In order to verify the global quantities in the cavity flow, the kinetic energy, E, is evaluated as:

$$E = \frac{1}{2}\int_{\Omega} ||U||^2 dx, \tag{8}$$

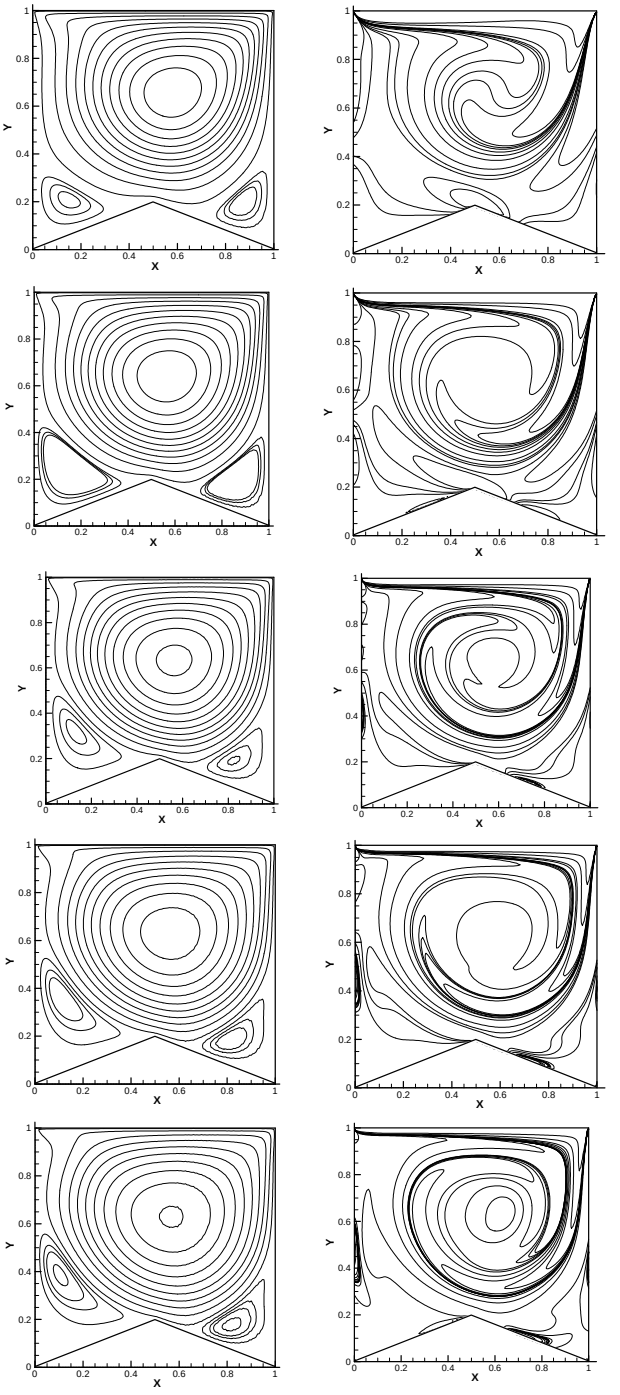
Y
X
0
0.2
0.4
0.6
0.8
1

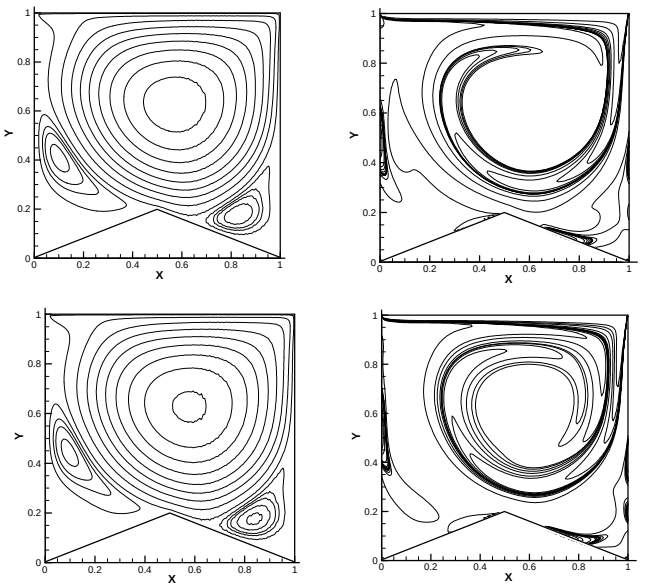

Figure 6: Streamlines and vorticity contours, respectively, for Reynolds numbers of 500 to 6000.

where $U_{i,j} = (u_{i,j}, v_{i,j})$. In a cavity flow the kinetic energy represents the total energy obtained by the system with the displacement. Global analysis of the flow also involves the entropy, Z, defined as:

$$Z = \frac{1}{2} \int_{\Omega} ||\zeta||^2 dx, \tag{9}$$

Table 3 shows the flow properties with increasing Reynolds number from 500 to 6000, where the maximum and minimum stream function, the vorticity in the same position as the maximum stream function, the total kinetic energy and the entropy are shown, along with the respective position at which these values were obtained.

Table 3 shows that the maximum values for the stream function, ψ_{max}, and vorticity, ζ, occur in the middle of the center of the primary vortex, while the minimum values for the stream function, ψ_{min}, occur closer to the bottom of the cavity, i.e., the position of the minimum stream function is the center of the secondary vortex, generated by the fluid recirculation on the bottom left or right of the cavity, according to the streamlines shown for Reynolds numbers of 500 to 6000 in Figure 6.

Our numerical results (see Table 3) suggest that the maximum stream function

Table 3: Proprieties of flow in irregular cavity, for $500 \leq Re \leq 6000$.

Re	Properties	Value	Location	
			x	y
500	ψ_{max}	0.1079	0.5800	0.6600
	ψ_{min}	-8.8911×10^{-4}	0.8800	0.2000
	ζ	2.5831	0.5800	0.6600
	E	0.0370		
	Z	9.3683		
1000	ψ_{max}	0.1072	0.5667	0.6400
	ψ_{min}	-2.3042×10^{-3}	0.1467	0.2600
	ζ	2.3766	0.5667	0.6400
	E	0.0376		
	Z	10.6111		
2000	ψ_{max}	0.1028	0.5600	0.6333
	ψ_{min}	-3.9447×10^{-3}	0.1267	0.3200
	ζ	2.1535	0.5600	0.6333
	E	0.0349		
	Z	11.9457		
3000	ψ_{max}	0.0966	0.5600	0.6333
	ψ_{min}	-4.8060×10^{-3}	0.1133	0.3600
	ζ	1.9835	0.5600	0.6333
	E	0.0315		
	Z	12.6767		
4000	ψ_{max}	0.0910	0.5600	0.6267
	ψ_{min}	-5.6171×10^{-3}	0.8200	0.1800
	ζ	1.8501	0.5600	0.6267
	E	0.0284		
	Z	13.1530		
5000	ψ_{max}	0.0862	0.5933	0.6267
	ψ_{min}	-6.4047×10^{-3}	0.2600	0.3600
	ζ	1.7400	0.5933	0.6267
	E	0.0258		
	Z	13.5077		
6000	ψ_{max}	0.0818	0.5933	0.6267
	ψ_{man}	-7.0052×10^{-3}	0.8333	0.1733
	ζ	1.6584	0.5933	0.6267
	E	0.0236		
	Z	13.8553		

value at the center of the primary vortex, ψ, decreases as the Reynolds number increases, and its vorticity, ζ, shows a similar behavior. We can see that the total kinetic energy gives converged values and decreases with the Reynolds number while the entropy increases. The reduction of the kinetic energy is important, for example, at Re = 6000 a 64% reduction in the kinetic energy of occurs compared with Re = 500.

Table 4: Values used to plot the contours of the stream function.

Reynolds	Values			
500 and 1000	0.1	0.09	0.08	0.07
	0.06	0.05	0.04	0.03
	0.02	0.01	0.002	-0.00015
	-0.0004	-0.0006		
2000 and 3000	0.1	0.09	0.08	0.07
	0.06	0.05	0.04	0.03
	0.02	0.01	0.002	-0.001
	-0.0025	-0.0035		
4000 and 5000	0.09	0.08	0.07	0.06
	0.05	0.04	0.03	0.02
	0.01	0.002	-0.001	-0.0025
	-0.0035	-0.005		
6000	0.08	0.07	0.06	0.05
	0.04	0.03	0.02	0.01
	0.002	-0.001	-0.0025	-0.0035
	-0.005	-0.0065		

3.3 Streamlines and vorticity contours

Streamlines and vorticity contours, in the steady state, are reported in Figure 6 for Re = 500, 1000, 2000, 3000, 4000, 5000 and 6000. The values used to plot the contours for the stream function and vorticity are listed in Tables 4 and 5, respectively. Note that for all Reynolds numbers investigated the steady state consists of one main vortex, a secondary vortex and a tertiary vortex, as seen in Figure 6. However, it is likely that other small vortices were formed near the bottom of the cavity, which were not captured with the methodology used. The size of the vortices is also dependent on the Reynolds number. In the bottom of the irregular cavity a major vortex occupies the central part of the domain, while minor vortices appear at the lower corners, and small vortices are probably formed in the top-left region as the Reynolds number increases.

Table 5: Values used to plot the contours of the vorticity.

Reynolds	Values			
500 and 1000	7	5	3	2.7
	2.6	2.5	2.3	2
	1.5	0.5	-0.15	-0.5
	-1.5	-2.3		
2000 and 3000	10	6	3.5	3
	2.3	2.2	2.18	2.16
	2	1.9	1.5	-0.13
	-1.5	-2.5		
4000 and 5000	10	5	3	2.5
	2.2	2	1.9	1.88
	1.86	1.85	1.84	1.5
	0.5	-2		
6000	8	5.5	4	2.5
	2	1.9	1.8	1.75
	1.72	1.70	1.65	1.5
	1.3	0.2		

Figure 6 also shows that the primary vortex is not significantly influenced by an increase in the Reynolds number, however, the small vortex on the left changes with this parameter. In the case of the irregular cavity, as the Reynolds number increases the vortices developing at the bottom grow, slowly pushing the main vortex to the right part of the cavity.

The values used to plot the stream function contours are listed in Table 4. These values are presented from the primary vortex center toward the boundaries and are given in decreasing order. The values used to plot the vorticity contours are described from top to bottom in Table 5.

4 Conclusions

In this paper, a two-dimensional analysis of the flow in a lid-driven irregular cavity is presented for Reynolds numbers of 500 to 6000, with the principal objective of collecting information on the steady viscous flow in a new irregular cavity. The computational code using the Eulerian-Lagrangian methodology was sufficiently robust to solve the flow within irregular regions. New results were obtained for the stream function, vorticity, kinetic energy and entropy. The evolution of the flow with an increase in the Reynolds number was analyzed and the maximum

and minimum stream functions were found to decreases with increasing Reynolds number. Meanwhile, there was a reduction in the vorticity function value at the maximum stream function point. With an increase in the Reynolds number there is less influence on the primary vortex, however, there is the creation of new eddies in the bottom left part of the cavity due to an increase in the secondary vortex velocity. These eddies rotate in the opposite direction and reduce the total energy of the flow observed, decreasing the kinetic energy with an increase in the Reynolds number.

References

Ahrem, R.; Beckert, A., Wendland, H. (2006): A meshless spatial coupling scheme for large-scale fluid-structure interaction problems. *CMES: Computer Modeling in Engineering & Sciences*, Vol 12, No. 2, pp. 121-136.

Arefmanesh, A.; Najafi, M.; Abdi, **H.** (2008): Meshless local Petrov-Galerkin method with unity test function for non-isothermal fluid flow. *CMES*: *Computer Modeling in Engineering & Sciences*, Vol. 25, No. 1, pp. 9-22.

Arefmanesh, A.; Najafi, M.; Nikfar, M. (2010): Meshless Local Petrov-Galerkin Simulation of Buoyancy-Driven Fluid Flow and Heat Transfer in a Cavity with Wavy Side Walls. *CMES*: *Computer Modeling in Engineering & Sciences*, Vol. 62, No. 2, pp.113-149.

Atluri S. N.; Liu H. T.; Han Z. D. (2006a): Meshless Local Petrov-Galerkin (MLPG) Mixed Finite Difference Method for Solid Mechanics. *CMES: Computer Modeling in Engineering & Sciences*, 15 (1)1-16.

Atluri S. N.; Liu H. T.; Han Z. D. (2006b): Meshless Local Petrov-Galerkin (MLPG) Mixed Collocation Method for Elasticity Problems. *CMES: Computer Modeling in Engineering & Sciences*, 14 (3) 141-152.

Basak, T.; Aravind, G.; Roy, S. (2009): Visualization of heat flow due to natural convection within triangular cavities using Bejan's heatline concept. *International Journal of Heat and Mass Transfer*, Vol. 52, pp. 2824-2833.

Batchelor, G. K. (1956): On steady laminar flow with closed streamlines at large Reynolds number. *J. Fluid Mech.*, Vol. 1, pp. 177-190.

Benjamin A. S.; Denny V. E. (1979): On the convergence of numerical solutions for 2-D flows in a cavity at large Re. *Journal of Computational Physics*, Vol. 33, pp. 340-358.

Botella, O.; Peyret, R. (1998): Benchmark spectral results on the lid–driven cavity flow. *Computers & Fluids*, Vol. 27, No. 4, pp. 421–433.

Bruneau, C.-H.; Saad, M. (2006): The 2D lid-driven cavity problem revisited. *Computers & Fluids*, Vol. 35, No. 3, pp. 326-348.

Chang, M.H.; Cheng, C.H. (1999): Predictions of lid-driven flow and heat transfer in an arc-shape cavity, *Int. Commun. Heat Mass Transf.*, Vol. 26, 829–838.

Chantasiriwan, S. (2006): Performance of multiquadric collocation method in solving lid-driven cavity flow problem with low Reynolds number. *CMES*: *Computer Modeling in Engineering & Sciences* Vol. 15, No. 3, pp. 137-146.

Chen, C.L.; Cheng, C.H. (2009)**:** Numerical study of the effects of lid oscillation on the periodic flow pattern and convection heat transfer in a triangular cavity. *International Communications in Heat and Mass Transfer* Vol 36, pp. 590-596.

Chen, C.L.; Cheng, C.H. (2002): Buoyancy-induced flow and convection heat transfer in an inclined arc-shape enclosure, *Int. J. Heat Fluid Flow*, Vol. 23, 823–830.

Darr, J. H.; Vanka, S. P. (1991): Separated flow in a driven. trapezoidal cavity. *Phys. Fluids A*, Vol. 3, No. 3, pp. 385-392.

Ding, H.; Shu, C.; Yeo, K. S.; Xu, D. (2006): Numerical computation of three-dimensional incompressible viscous flows in the primitive variable form by local multiquadratic differential quadrature method. *Comp. Methods in Appl. Mech. Engr.*, Vol. 195, No. 7-8, pp. 516-533.

Duan, Y.; Liu, R. (2007): Lattice Boltzmann simulations of triangular cavity flow and free-surface problems. *Journal of Hydrodynamics*, Vol. 19, No. 2, pp. 127-134.

Ghia, U.; Ghia, K. N.; Shin, C. T. (1982): High-re solutions for incompressible flow using the Navier-Stokes equations and multigrid method. *J. Comp. Phys.*, Vol. 48, pp. 387-411.

Glowinski, R.; Guidoboni, G.; Pan, T. –W. (2006): Wall-driven incompressible viscous flow in a two-dimensional semi-circular cavity. *Journal of Computational Physics*, Vol. 216, No. 1, pp. 76-91.

Grimaldi A.; Pascazio G.; Napolitano M. (2006): A parallel multi-block method for the unsteady vorticity-velocity equations. *CMES: Computer Modeling in Engineering & Sciences*, Vol 14, No. 1, pp. 45-56.

Han Z. D.; Liu H. T.; Rajendran A. M.; Atluri S. N. (2006): The Applications ofMeshless Local Petrov-Galerkin (MLPG) Approaches in High-Speed Impact, Penetration and Perforation Problems. *CMES: Computer Modeling in Engineering & Science*s, 14 (2) 119-128.

Jyotsna, R.; Vanka, S. P. (1995): Multigrid calculation of steady, viscous flow in a triangular cavity. *Journal of Computational Physics*, Vol. 122, No. 1, pp. 107-117.

Kaluri, R. S.; Anandalakshmi, R.; Basak, T. (2010): Bejan's heatline analysis of natural convection in right-angled triangular enclosures: Effects of aspect-ratio and

thermal boundary conditions. *International Journal of Thermal Sciences*, Vol. 49, pp. 1576-1592

Li, M.; Tang, T. (1996): Steady viscous flow in a triangular cavity by efficient numerical techniques. *Computers Math. Applic.*, Vol. 31, No. 10, pp. 55-65.

Lin, H.; Atluri, S. N. (2001): The meshless local Petrov-Galerkin (MLPG) method for solving incompressible Navier-Stokes equations. *CMES: Computer Modeling in Engineering & Sciences*, Vol. 2, No. 2, pp. 117-142.

Mai-Duy, N.; Mai-Cao, L.; Tran-Cong, T. (2007): Computation of transient viscous flows using indirect radial basis function networks. *CMES: Computer Modeling in Engineering & Sciences*, Vol. 18, No. 1, pp. 59-78.

Mai-Cao, L.; Tran-Cong, T. (2008): A meshless approach to capturing moving interfaces in passive transport problems. *CMES: Computer Modeling in Engineering & Sciences*, Vol. 31, No. 3, pp. 157-188.

Mai-Duy N.; Tran-Cong T. (2004): Boundary integral-based domain decomposition technique of Navier-Stokes equations. *CMES: Computer Modeling in Engineering & Sciences*, Vol. 6, No. 1, pp. 59-75.

Mai-Duy N.; Tran-Cong T. (2009): A Cartesian-Grid Discretisation Scheme Based on Local Integrated RBFNs for Two-Dimensional Elliptic Problems. *CMES: Computer Modeling in Engineering & Sciences*, Vol. 51, No. 3, pp. 213-238.

Mariani, V. C; Alonso, E. E. M., Peters, S. (2008): Numerical results for a colocated finite-volume scheme on Voronoi meshes for Navier-Stokes equations. *CMES: Computer Modeling in Engineering & Sciences*, Vol. 29, No. 1, pp. 15-27.

Mariani, V. C.; Prata, A. T. (2008): A Eulerian-Lagrangian method applied to fluid flow in lid-driven cavities with irregular bottom walls. *Numer. Heat Transfer Part B*, Vol. 53, No. 3, pp. 1-28.

Mariani, V. C.; Prata, A. T.; Deschamps, C. J. (2010): Numerical analysis of fluid flow through radial diffusers in the presence of a chamfer in the feeding orifice with a mixed Eulerian–Lagrangian method. *Computers & Fluids* Vol 39, pp. 1672-1684.

McQuain, W. D.; Ribbens, C. J.; Wang, C.-Y.; Watson, L. T. (1994): Steady viscous flow in a trapezoidal cavity. *Comput. Fluids*, Vol. 23, No. 4, pp. 613-626.

Moffatt H. K. (1963): Viscous and resistive eddies near a sharp corner. *J. Fluid Mech.*, Vol. 18, No. 1, pp. 1-18.

Nicolás, A.; Bermúdez, B. (2004): 2D Incompressible viscous flows at moderate and high Reynolds numbers. *CMES: Computer Modeling in Engineering & Sciences*, Vol. 6, No. 5, pp. 441-451.

Nicolás A.; Bermúdez, B. (2007): Viscous incompressible flows by the velocity-

vorticity Navier-Stokes equations. *CMES: Computer Modeling in Engineering & Sciences*, Vol 20, No. 2, pp. 73-83.

Orsini, P.; Power, H.; Morvan, **H.** (2008): Improving volume element methods by meshless radial basis function techniques**.** *CMES: Computer Modeling in Engineering & Sciences*, Vol. 23, No. 3, pp. 187-207.

Pasquim, B. M.; Mariani, V. C. (2008): Solutions for Incompressible Viscous Flow in a Triangular Cavity using Cartesian Grid Method. *CMES: Computer Modeling in Engineering & Sciences*, Vol. 35, No. 2, pp. 113–132.

Patankar, S. V. (1980): *Numerical heat transfer and fluid flow*, Hemisphere Publishing Corporation, USA.

Ribbens, C. J.; Wang, C. Y.; Watson, L. T.; Alexander, K. A. (1991): Vorticity induced by a moving. elliptic belt. *Comput. Fluids*, Vol. 20, No. 2, pp. 111-119.

Ribbens, C. J.; Watson, L. T.; Wang, C. –Y. (1994): Steady viscous flow in a triangular cavity. *J. Comput. Phys.*, Vol. 112, pp. 173-181.

Saha, S. C. (2011): Unsteady natural convection in a triangular enclosure under isothermal heating. *Energy and Buildings*, Vol. 43, pp. 695–703.

Sellountos, E. J.; Sequeira, A. (2008): A hybrid multi-region BEM/LBIE-RBF velocity-vorticity scheme for the two-dimensional Navier-Stokes equations. *CMES: Computer Modeling in Engineering & Sciences*, Vol. 23 No. 2, 127-147.

Shan, Y. Y.; Shu, C.; Lu, Z. L. (2008): Application of Local MQ-DQ Method to solve 3D incompressible viscous flows with curved boundary.

Shyy, W.; Udaykumar, H. S.; Rao, M. M.; Smith, R. W. (1996): Computational Fluid Dynamics with Moving Boundaries, Taylor & Francis, UK. *CMES: Computer Modeling in Engineering & Sciences*, Vol. 25, No. 2, 99-113.

Tsai, C.; Young, D.L.; Cheng A.H. (2002): Meshless BEM for Three-Dimensional Stokes Flows. *CMES: Computer Modeling in Engineering & Sciences*, Vol. 3, No. 1, 117-128.

Udaykumar, H. S.; Shyy, W.; Rao, M. M. (1996): ELAFINT: A mixed Eulerian-Lagrangian method for fluid flows with complex and moving boundaries. *Int. J. Numerical Methods in Fluids*, Vol. 22, No. 8, pp. 691-712.

Vynnycky, M.; Kimura, S. (1994): An investigation of recirculating in a driven cavity. *Phys. Fluids A*, Vol. 6, No. 11, pp. 3610-3620.

Wen, P. H.; Hon, Y. C. (2007): Geometrically Nonlinear Analysis of Reissner-Mindlin Plate by Meshless Computation. *CMES: Computer Modeling in Engineering & Scienc*es, Vol. 21, No. 3, pp. 177-192.

Ye, T.; Mittal, R.; Udaykumar, H. S.; Shyy, W. (1999): An accurate Cartesian

grid method for viscous incompressible flows with complex immersed boundaries. *J. Comp. Phys.*, Vol. 156, No. 2, pp. 209-240.

Young, D. L.; Lane, S. C.; Lin, C. Y.; Chiu, C. L.; Chen, K. C. (2004): Solutions of 2D and 3D Stokes laws using multiquadrics method. *Engr. Anal. With Bound. Elem.*, Vol. 28, No. 10, pp. 1233-1243.